BIODIVERSITAS
Volume 25, Number 10, October 2024
Pages: 3899-3908

ISSN: 1412-033X
E-ISSN: 2085-4722
DOI: 10.13057/biodiv/d251050

Structural stability analysis of rain trees (*Samanea saman*) subjected to dead, live, and wind loads combination

SITI CHUROTUL AINI[1], ULFA ADZKIA[1,2], EFFENDI TRI BAHTIAR[1], M. MIFTAH RAHMAN[1,3], AGUS BUONO[4], LINA KARLINASARI[1,♥]

[1]Department of Forest Products and Technology, Faculty of Forestry and Environment, Institut Pertanian Bogor. Jl. Ulin Lingkar Akademik, Dramaga, Bogor 16680, West Java, Indonesia. Tel.: +62-251-862-1677, Fax.: +62-251-862-1256, ♥email: karlinasari@apps.ipb.ac.id
[2]Faculty of Agriculture and Forestry, Universitas Sulawesi Barat. Jl. Hasanuddin, Majene 91412, West Sulawesi, Indonesia
[3]Department of Sustainable Bioproducts, Forest and Wildlife Research Center (FWRC), Mississippi State University. 775 Stone Blvd., Mississippi State 39759, Starkville, USA
[4]Department of Computer Science, Faculty of Mathematics and Natural Sciences, Institut Pertanian Bogor. Jl. Meranti, Kampus IPB Dramaga, Bogor 16680, West Java, Indonesia

Manuscript received: 25 July 2024. Revision accepted: 29 October 2024.

Abstract. *Aini SC, Adzkia U, Bahtiar ET, Rahman MM, Buono A, Karlinasari L. 2024. Structural stability analysis of rain trees* (Samanea saman) *subjected to dead, live, and wind loads combination. Biodiversitas 25: 3899-3908.* Tree failure can arise from factors associated with load resistance and structural stability at sites of environmental growth. In this study, an investigation was conducted into the structural analysis of standing trees, considering the combination of compression and flexure loads in the adoption of building code guidelines. The objective of this study is to determine the safety factor based on a combined load combination governing the Euler and Ylinen Buckling Stress Method. The study used 50 rain trees (*Samanea saman* (Jacq.) Merr.). Therefore, to assess the impact of various load combinations on standing trees, including dead, live, and wind loads, three analyses were performed: (1) D + L + W, (2) D + L, and (3) D only. The dead load (D) represents the weight of the crown and stem above the observed section, the live load (L) accounts for activities such as climbing or hanging, and W represents wind loads. The D + L + W load combination induced both compression and bending stresses on the trees, whereas the D + L and D only focused on compression loads. Determining the minimum critical height is crucial in assessing the safety factor and categorizing trees into three groups: unsafe, safe, and very safe. The results indicated that the combined load of D + L + W demonstrated that the minimum critical height resulted from the superposition of compression and bending stresses. This finding underscores the significant role of the wind in the safety of standing trees. Structural stability analysis revealed that 18 trees were unsafe, 30 were safe, and 2 were classified as very safe. This research contributes valuable insights into understanding tree biomechanics and tree characteristics, offering a distinct approach compared to existing methods.

Keywords: Combined load, critical height, environment, safety factor, tree stability

INTRODUCTION

One of the causes of tree failure is the instability of the tree structures. Tree stability depends on an analysis of the physical and mechanical conditions of the tree (Dahle et al. 2014; Linhares et al. 2021) is a key aspect that urban planners need to consider. Analysis of physical condition includes morphological characteristics of the stem, crown, tree architecture, and roots (Karlinasari et al. 2021). Meanwhile, in mechanical condition analysis, load analysis includes the analysis of forces acting on the tree, such as dead loads (own weight), live loads due to external forces, and wind loads (Miyashita and Suzuki 2021). Assuming a tree is a rod structure, the National Design Specification (AWC 2018) can be used to analyze the tree trunk. The National Design Specification (AWC 2018) explains that load calculations, whether combined or individual, are differentiated based on the value of the load duration factor (C_D) used, where the largest C_D value is obtained for each load combination analyzed. Load combinations are combinations of loads acting on a tree, such as combinations of compression and bending loads and internal and external compression loads. Combining these forces can result in flexural stress and bending stress in the tree trunk. Trees respond differently to various pressures occurring upon them, including wind loads. According to Moore et al. (2018), trees react to loads greater than their structural capability via little movements of their leaves, branches, and trunks, ultimately leading to trunk failure. When a tree is in a sloping environment, it may also respond in another way, such as by creating reaction wood to help it stand back up (Fournier et al. 2013; Badel et al. 2015). This shows that a comprehensive understanding of tree stability matters for an urban region since it impacts community safety and infrastructure (Rahardjo et al. 2014).

Trees planted along road greenways usually serve as shade providers, identity markers, temperature regulators, noise dampeners, air purifiers, carbon absorbers, soil conservers, environmental preservatives, and aesthetic enhancers (Jansson 2014; Li et al. 2016; Tiwary et al. 2016; O'Brien et al. 2017; Wolf et al. 2020). Basically, street trees, usually as a shading trees, represent a long-term investment for regulating the microclimate (Horváthová et al. 2021). Tree types can be the key to selecting shade trees. Afrianto et al. (2021) reported that tree species from Family of Fabaceae are dominant as urban tress with the

atribut of tree crown as well as branches aspects became a consideration for selecting the tree species According to the Directorate General of Highways (1996) in Indonesia, shaded trees have a minimum branch height of 2 m above the ground, a non-drooping branch shape, dense leaf mass, are planted in rows, and can provide shade to pedestrians by blocking direct sunlight. Rain trees/*Trembesi* (*Samanea saman* (Jacq.) Merr) are known as shading trees with the crown form as an umbrella. Rain trees can reach heights of 15-25 m with a spreading crown type that can achieve a crown width of up to 30 m when planted in spacious and open areas (Karlinasari et al. 2021). *Trembesi* (*S. saman*) has dominant lateral branches that spread at the same level, and this growth pattern is referred to as characteristic of the decurrent tree (Coder 2014). This tree is one of the most adaptable to less-than-ideal environmental conditions (Ow and Ghosh 2017; Ow and Yusof 2018). This study was conducted on rain trees which have become favorite trees because of their shape so that known as shade trees in tropical areas. Research that takes into account external loads from wind is very interesting because its influence is often not taken into account seriously.

Study by Karlinasari et al. (2023) has focussed on self-weight-loading rain trees. By using the paraboloid geometric model to approach the crown characteristics of the excurrent tree and the paraboloid duo geometric model to approach the crown characteristics of the decurrent tree. This study successfully develop the safety factor of urban trees growing in a built environment as modelled following the SNI 7973 (2013). According to this research, considering internal and external aspects will make the model more thorough. Studi by Fathi (2020) mentioned that there was a relationship between static loading and the dynamic response of the tree due to environmental influences in studying tree stability. His study also explored characteristics of roots that caused uprooting in terms of being affected by a force in the tree. Research by Jackson et al. (2020) indicates that taller trees are less likely to break under gravity or their own weight, mainly due to the tree's architecture rather than its material properties. Conversely, the likelihood of wind damage grows with height despite the greater trunk diameters. The wind is a crucial factor influencing the structural stability of trees, as its wind load causes bending stress on stem trees (ver Planck and MacFarlane 2019). This is evidenced by instances of strong winds causing fallen trees, which can direct risks to the public, including property damage, traffic disruption, and threats to human life (Hui et al. 2022). Based on this background, this study aimed to analyze the structural stability and resistance of the rain tree (*S. saman*) when subjected to a combination of dead, live, and wind loads, and the safety factor of the standing trees was determined. In this study we do not include the affect of root characteristic as a factor affecting tree stability in responding on the forces on the trees.

MATERIALS AND METHODS

Selection of target trees

The observed trees consisted of 50 planted rain trees in Institut Pertanian Bogor, Bogor, West Java, Indonesia (Figure 1) with a single main stem, without considering the health conditions of the trees, as referred to in the study by Karlinasari et al. (2023).

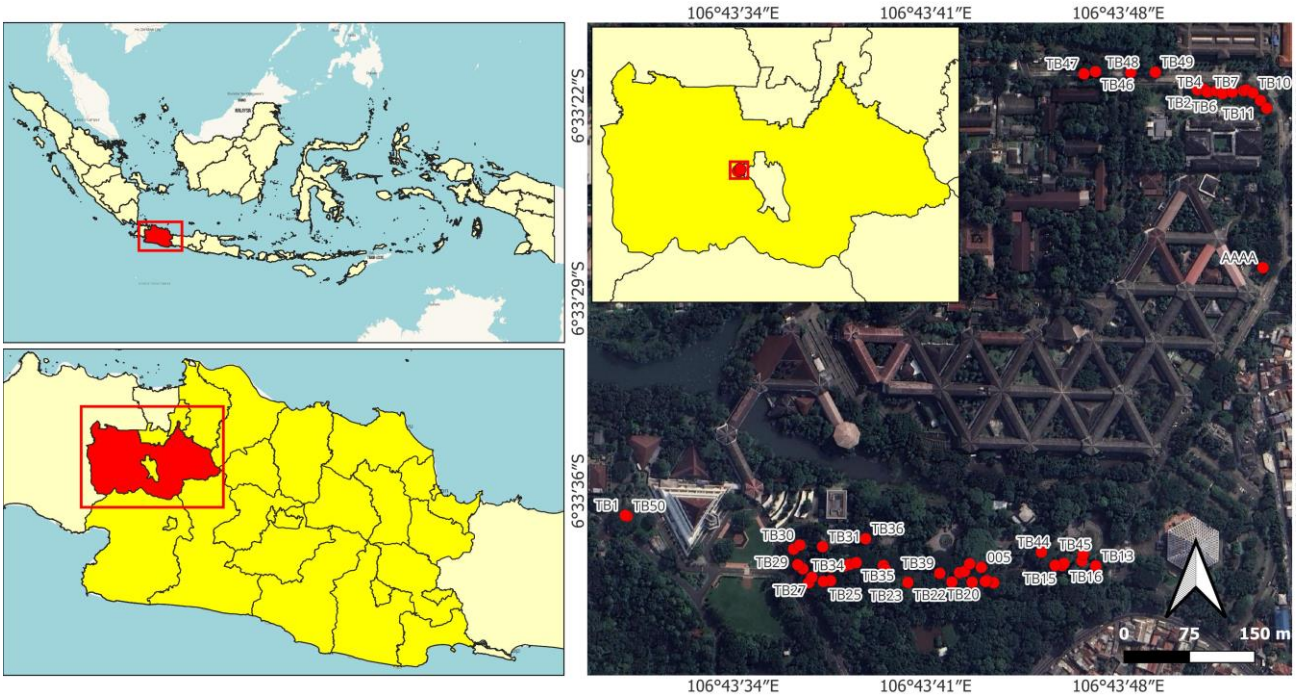

Figure 1. Location of target trees in Institut Pertanian Bogor, Bogor, West Java, Indonesia

Procedures

Measurement and determination of tree characteristics

Tree characteristics were evaluated based on tree morphometric measurements consisting of diameter at breast height (D_{bh}), tip diameter (D_{tr}), crown diameter (D_c), total tree height (H), branch-free height (H_{tbc}), crown height (H_c), and lowest crown height (H_{ck}) as shown in Figure 2, while longest crown diameter (d_1), and shortest crown diameter (d_2) (Karlinasari et al. 2021, 2023) as shown in Figure 3. D_{bh} was measured using a diameter tape (Iizuka et al. 2018), and D_{tr} was measured using the Spiegel Relascope Bitterlich (SRB) (Palace et al. 2015). The tree height was measured using a haga hypsometer (Němec 2015). Crown diameter measurements were taken along the dripline in eight directions to obtain the longest and shortest crown diameters, as depicted in Figure 3 as stipulated by Ow et al. (2019). Other parameters of tree morphometrics include taper (T) and slenderness (S) (Karlinasari et al. 2023). Stem tapering was calculated using Equation 1, which was derived from the difference between the diameter at breast height (D_{bh}) and diameter at the tip (D_{tr}) divided by the diameter at breast height (D_{bh}). Stem slenderness was calculated by dividing the branch-free height (H_{tbc}) by D_{bh} (Telewski and Moore 2016) (Equation 2).

$$T = \frac{D_{bh} - D_{tr}}{D_{bh}} \quad (1)$$

$$S = \frac{H_{tbc}}{D_{bh}} \quad (2)$$

Determination of compression stress of standing trees

In analyzing the stability of a structure, it is necessary to consider the forces acting on the tree, such as compression and bending stress. In a standing tree, the compression load comprises internal loads due to self-weight loading of stem weight and crown weight and external compression loads, such as the weight of a person climbing a tree to its maximum height at the branch-free height (H_{tbc}). The determination of external compression load (P) refers to the weight of Indonesian adult males aged 19-28 years, ranging between 34.8-107.7 kg with an average of 67 kilograms (Mulyasari and Purbowati 2018). Following a study by Karlinasari et al. (2023), the stem weight and crown weight are determined based on wood density multiple stem volume and crown density multiple crown volume, respectively. The tree crown geometry model used was a paraboloid duo type-I shape, as shown in Figure 4. In a standing tree, the compression load generated by the crown is limited to the crown's weight above the imaginary line at the x-point. Meanwhile, wood density was obtained from a small core sample and determined as stipulated by ASTM D-2395 (2017), ensuring the reliability of our methods. In comparison, crown density was used to reference (1.9 kg m^{-3}) from a previous study, as mentioned by Karlinasari et al. (2023).

The stem volume was determined using the Greenhill method, which was explained by considering the stem geometric model of the hooked cone (Karlinasari et al. 2023). Meanwhile, the crown volume of the rain tree was calculated using the geometric crown model of paraboloid duo type I, referring to the diameter and crown height. Simulation calculation of the x-imaginary line position using the functions in Equation 3 and determination of the crown volume using the function in Equation 4. Both entered the online application Desmos Graphic Calculator.

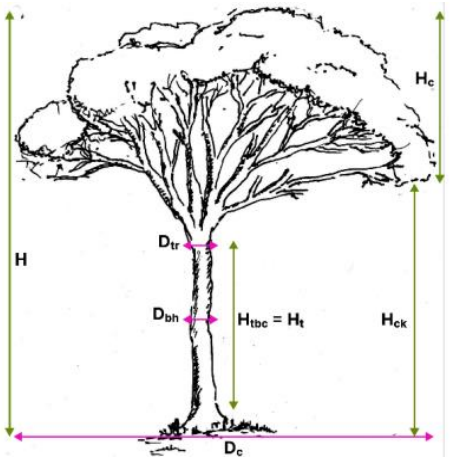

Figure 2. Measurement of tree morphometric

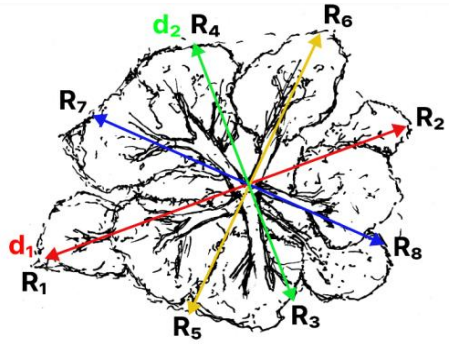

Figure 3. Top-view crown measurement of trees. Notes: R_1 direction of the longest crown; R_2 opposite direction of the longest crown; R_3 direction of the shortest crown; R_4 opposite direction of the shortest crown; R_5, R_6, R_7, and R_8, four directions between the longest and shortest canopies; d_1 longest crown diameter; and d_2 shortest crown diameter

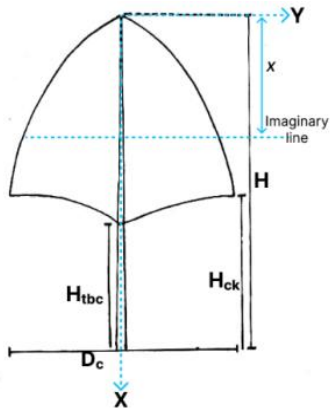

Figure 4. Geometric model of tree-crown paraboloid duo type I: $H_{tbc} \leq H_{ck}$ (Karlinasari et al. 2023)

$$x = \begin{cases} 4\left(\frac{H-H_{ck}}{D_c^2}\right)y^2 & \text{for } 0 \le x \le H-H_{ck} \\ -\left(\frac{H_{tbc}-H_{ck}}{\left(\frac{D_c}{2}\right)^2}\right)y^2 + 2\left(\frac{H_{tbc}-H_{ck}}{\left(\frac{D_c}{2}\right)}\right)y + H - H_{tbc} & \text{for } 0 \le y \le \frac{D_c}{2} \\ -\left(\frac{H_{tbc}-H_{ck}}{\left(\frac{D_c}{2}\right)^2}\right)y^2 - 2\left(\frac{H_{tbc}-H_{ck}}{\left(\frac{D_c}{2}\right)}\right)y + H - H_{tbc} & \text{for } -\frac{D_c}{2} \le y \le 0 \end{cases} \quad (3)$$

$$V_{ca} = \begin{cases} \frac{\pi}{8}\left(\frac{D_c^2 x^2}{H-H_{ck}}\right) \text{for } 0 \le x \le H-H_{ck} \\ \frac{\pi D_c^2(-H+H_{ck}+x)\left(8H_{tbc}\sqrt{\frac{-H+H_{ck}+x}{H_{ck}-H_{tbc}}} - 8Hck\sqrt{\frac{-H+H_{ck}+x}{H_{ck}-H_{tbc}}} - 6H_{tbc} - 3H + 9H_{ck} + 3x\right)}{24(H_{ck}-H_{tbc})} + \frac{\pi}{8}D_c^2(H-H_{ck}) \\ \text{for } H-H_{ck} \le x \le H-H_{tbc} \\ \frac{\pi}{24}D_c(3H-2H_{ck}-H_{tbc}) \text{for } x \ge H-H_{ck} \end{cases} \quad (4)$$

The actual compression stress ($G(x)$) (Equation 5) consists of the internal load (stem weight (P_{bx}), crown weight (P_{cx})), external load (P), and effective surface area (A_{ef}) (Equation 6). The external load is the weight of a worker who is climbing the tree.

$$G(x) = \frac{P + P_{bx} + P_{cx}}{A_{ef}} \quad (5)$$

$$A_{ef} = \frac{\pi}{4} D_{ef}^2 \quad (6)$$

The allowable compression stress (F_c), based on the Euler-Ylinen buckling stress analysis formula, was used in the study on the critical buckling height, as pointed out in Equation 7 (Karlinasari et al. 2023). This formula was applied to calculate the compression stress generated by the National Design Standard (AWC 2018). It was obtained by dividing the lower limit of 5% (K_T) with a 95% confidence level) by the value of the adjustment factor to clear the wood properties and then multiplying by the parallel-to-grain compression strength (M_{cs}). K_T was derived from SNI 7973 (2013) as 1-1.645C_{ov}, where the coefficient of variation for the compression parallel-to-grain (C_{ovFc}) value is 0.18 obtained from the Forest Products Laboratory (2010). The adjustment factor for hardwood parallel-to-grain compression strength is 2.1, referring to ASTM D-245 (2002), while the parallel-to-grain compression strength (M_{cs}) value for the raintree follows the value as resulted by Puspitasari (2021) of 22.97 M_{Pa}.

$$F_c = \frac{(1 - 1.645 C_{ovFc})}{2.1} \times M_{cs} \quad (7)$$

The corrected allowable compression stress ($L(x)$) was calculated by multiplying F_c with various correction factors (AWC 2018). The correction factors used include load duration (C_D), wet service (C_M), temperature (C_t), critical section (C_{cs}), load sharing (C_{ls}), condition treatment (C_{ct}), incising (C_i), size (C_F), and column stability (C_p). For more detailed explanation regarding the correction factors, see AWC (2018). The correction factor values obtained from the AWC (2018) were 0.8, 1, 1, and 1 for C_M, C_t, C_{cs}, C_{ls}, C_{ct}, and C_i, respectively. The load duration (C_D) value depends on the applied load. If the applied load is only the internal load (dead load), the C_D value used is 0.9. However, if the applied load is a combination of internal and external loads (live load), the C_D value used is 1.25 (AWC 2018). The C_F values were obtained using Equation 8. The effective diameter (D_{ef}), stem diameter at ground level (D_b), diameter along the x line (D_x), and estimated tip diameter (D_h) are presented in Equations 9, 10, 11, and 12, respectively.

$$C_F = \left(\frac{12 \times 0.0254}{D_{ef} \times 100}\right)^{\frac{1}{9}} \quad (8)$$

$$D_{ef} = D_x + \frac{(D_b - D_x)}{3} \quad (9)$$

$$D_b = D_h + \frac{(D_{bh} - D_h)x}{(H - H_{dbh})} \quad (10)$$

$$D_x = D_h + \frac{(D_{bh} - D_h)x}{(H - H_{dbh})} \quad (11)$$

$$D_h = \frac{(H - H_{dbh})D_t - (H - H_t)D_{bh}}{H_t - H_{dbh}} \quad (12)$$

The column stability (C_p) value was obtained using Equation 13. To calculate C_p, supporting equations are required, such as the reference compression design value parallel to the grain multiplied by all applicable adjustment factors except C_p (P_{ck}) in Equation 14, critical buckling design value for compression members (P_{cE}) in Equation 15, effective inertial moment (I_{ef}) in Equation 16, effective length (l_{ef}) in Equation 17, adjusted modulus of elasticity for column stability calculation (E_{min}) in Equation 18, and bending stiffness factor (C_T) in Equation 19. The value of the effective length (l_{ef}) was adjusted using the coefficient of the buckling length (K_e). The value of the correction coefficient of the actual length with an effective length was 2.1, which was used with consideration of their support as a standing tree column referring to SNI 7973 (2013). The coefficient of variation for the modulus of elasticity (C_{ovE}) is 0.22 based on Forest Product Laboratory (2010), and the parameter non-linear for column or c value is 0.85. The bending stiffness factor (C_T) in which the calculation of the moisture content coefficient (K_M) used is 1200, and the effective length value (l_{ef}) is 96 (AWC 2018).

$$C_p = \frac{1 + \left(\frac{P_{cE}}{P_{ck}}\right)}{2c} - \sqrt{\left(\frac{1 + \left(\frac{P_{cE}}{P_{ck}}\right)}{2c}\right)^2 - \frac{\left(\frac{P_{cE}}{P_{ck}}\right)}{c}} \quad (13)$$

$$P_{ck} = F_C C_D C_M C_t C_{cs} C_{ls} C_{ct} C_i C_F 10^6 A_{ef} \quad (14)$$

$$P_{cE} = \frac{\pi^2 (C_M C_t C_{cs} C_{ls} C_{ct} C_i C_T E_{min} 10^6) I_{ef}}{l_{ef}^2} \quad (15)$$

$$I_{ef} = \frac{\pi}{64} D_{ef}^4 \quad (16)$$

$$l_{ef} = K_e(H - x) \quad (17)$$

$$E_{min} = \frac{1.03}{1.66}(1 - 1.645 C_{ovE})\, E_s \quad (18)$$

$$C_T = \begin{cases} 1 + \dfrac{K_M\left(\frac{l_{ef}}{0.00254}\right)}{K_T(E_s \times 145.038)} & \text{for } 0 < l_{ef} < 96 \times 0.0254 \\ 1 + \dfrac{K_M \times 96}{K_T(E_s \times 145.038)} & \text{for } l_{ef} \geq 96 \times 0.0254 \end{cases} \quad (19)$$

To determine the static modulus of elasticity (E_s) in the calculations *of* E_{min} and $C_{T,\ the}$ Modulus of Elasticity or Young's modulus (E) was used. This value is related to the characteristics of the material and the bending properties. The value of E was measured using non-destructive testing based on sound wave propagation (Urhan et al. 2014; Fundova et al. 2019; Schimleck et al. 2019). Non-destructive testing has been widely used in the forestry and urban tree industries to infer the physical and mechanical properties of wood (Gonçalves et al. 2020). A FAKOPP Microsecond Timer was used for this purpose. The obtained data consisted of the sound wave propagation time (t), which was generated along the tree stem (s), which was then calculated as the sound wave velocity (S_{WVT}) (see Equation 20). It was used to determine the static modulus of elasticity (E_s) according to the calculation by Duong et al. (2022) in Equation 21. Equation 22 provides the mathematical formula for the corrected parallel-to-grain allowable compression stress ($L(x)$).

$$S_{WVT} = \frac{s}{t} \quad (20)$$

$$E_s = 0.004\ S_{WVT} - 6.127 \quad (21)$$

$$L(x) = F_C\, C_D C_M C_t C_{cs} C_{ls} C_{ct} C_i C_F C_P 10^6 \quad (22)$$

Determination of bending stress of standing trees

Spatz and Bruechert (2000) explain that actual bending stress (f_b) occurs when a tree is subjected to wind load. The mathematical determination of the wind load on a tree is presented in Equation 23. The air drag coefficient (C_d) value is 0.2, and the air density (ρ_a) value used was the standard atmospheric temperature and pressure of 1.226 kg m^{-3} (ISO 2533 1975). The wind speed (v_w) value used was the average maximum wind speed in the site location (Bogor, West Java, Indonesia) in 2022, which was 9-10 m s^{-1} (BPS 2022). The area of vertical crown projection (A_{cr}) was calculated using Equation 24. Based on the Beaufort scale, the wind speed is category number 5, with a description of a fresh breeze characterized by a smaller tree sway (Cardia and Lovatelli 2015). In contrast, mainland Europe (subtropical regions) has higher wind speeds than Indonesia (tropical regions), such as Poland, ranging from 20-30 m s^{-1}, about 30-32 m s^{-1} in Latvia, and 26 m s^{-1} in Hungary, depending on the region (Kadry et al. 2019). In previous studies, many authors report that the air drag coefficient decreases with increases in wind velocity and becomes constant at high wind speeds (Kitagawa et al. 2015; Gardiner et al. 2016; Koizumi et al. 2016; Borisevich and Vikhrenko 2018; Manickathan et al. 2018; Moore et al. 2018).

$$P_w = \frac{1}{2}\, C_d\, A_{cr}\, \rho_a\, v_w^2 \quad (23)$$

$$A_{cr} = \frac{(2H - H_{cK} - H_{tbc})\, D_c}{3} \quad (24)$$

Equation 25 obtained the actual bending stress (f_b) values. Equations 26, 27, 28, 29, and 30 are supporting equations used to calculate the f_b value, i.e., centroid crown (C_{cr}), first momen crown (Q_{cr}), centroid (c_s), diameter wind point (D_w), and diameter along the crown (D_{cr}), respectively.

$$f_b = \frac{M_{wmaks} \times c_s}{I_{efw}} = \frac{(P_w \times (H - c_{cr})) \times c_s}{\frac{\pi}{64} D_w^4} \quad (25)$$

$$c_{cr} = \frac{Q_{cr}}{A_{cr}} \quad (26)$$

$$Q_{cr} = \frac{2D_c}{5}(H - H_{cK})^2 + D_c\left(\frac{1}{2}(2H - H_{tbc} - H_{cK})(H_{cK} - H_{tbc}) - \int_{H-H_{cK}}^{H-H_{tbc}} \left(x\sqrt{\frac{(H - H_{cK} - x)}{(H_{tbc} - H_{cK})}}\right) dx\right) \quad (27)$$

$$c_s = \frac{1}{2} D_w \quad (28)$$

$$D_w = \frac{1}{3}(D_{cr} + D_b) \quad (29)$$

$$D_{cr} = D_h + \frac{(D_{bh} - D_h) c_{cr}}{(H - H_{dbh})} \quad (30)$$

The allowable bending stress (F_b), mathematically expressed in Equation 31, is derived by dividing the lower limit of 5% ((K_T) with a 95% confidence level) by the value of the adjustment factor to clear the wood properties and then multiplying by the Modulus of Rupture (MoR). K_T was derived from SNI 7973 (2013) as 1-1.645C_{ov}, where the coefficient of variation for the modulus of rupture (C_{ovMoR}) value was 0.16, as obtained from the Forest Product Laboratory (2010). The adjustment factor for the hardwood bending strength was 2.3 (ASTM D-245 2002). The MoR value for the rain tree is 39.15 MPa (Puspitasari 2021).

$$F_b = \frac{(1 - 1.645 C_{ovMoR})}{2.3} \times MoR \quad (31)$$

The corrected allowable bending stress (M_x) was calculated by multiplying F_b with several correction factors. The correction factors used included load duration (C_{Db}), wet service (C_{Mb}), temperature (C_{tb}), flat use (C_{fub}), repetitive members (C_{rb}), condition treatment (C_{ctb}), incising (C_{ib}), size (C_{Fb}), and beam stability (C_{Lb}). The correction factor values obtained from AWC (2018) are 0.85 for C_{Mb}, 1 for C_{tb}, 1 for C_{fub}, 1 for C_{rb}, 1 for C_{ctb}, 1 for C_{ib}, 1 for C_{Fb}, and 1 for C_{Lb} (as trees cannot twist). *The* C_{Db} value depends on the applied load (explained in more detail in subsection 2.6). The formula for the corrected allowable bending stress (M_x) is mathematically expressed as Equation 32.

$$M_x = F_b C_{Db} C_{Mb} C_{tb} C_{fub} C_{rb} C_{ctb} C_{ib} C_{Fb} C_{Lb} 10^6 \quad (32)$$

Determination of combined stress of standing trees

AWC (2018) explained that when both compression and bending loads act on a tree simultaneously, the calculation of the load conditions is divided into three categories. The first is a combination of compression and bending loads (D + L + W), the second is a combination of internal and external compression loads (D + L), and the third is an internal compression load only (D). The dead load (D) represents the weight of the crown and stem above the observed section, the live load (L) accounts for

activities such as climbing or hanging, and W represents wind loads. For those three categories, the load duration factor (C_D) values were different. The first (D + L + W), second (D + L), and third conditions (D) used C_D of 1.6, 1.25, and 0.9, respectively. The combination of the compression and bending stress values must be smaller than 1 (Equation 33). The parameters in this equation were explained in the previous subsection.

$$\left(\frac{G_{(x)}}{L_{(x)}}\right)^2 + \frac{f_b}{M_x\left[1-\left(\frac{G_{(x)}A_{ef}}{P_{cE}}\right)\right]} < 1.0 \quad (33)$$

Determination of critical height and tree safety factor

According to Karlinasari et al. (2023), the critical tree height (H_{cr}) can be used to determine the safety factor (S_f). The critical height of the tree was obtained through graphical-mathematical analysis. This graphical-mathematical analysis is obtained and simulated by entering most of the equations (Equations 3 until 33) into the Desmos Graphic Calculator software, free access (https://www.desmos.com/calculator?lang=id), considering the applied loads on the tree (load conditions), resulting in critical height values for each tree. Because the value of the stress calculated on each part will produce a large and continuous number, the graphical-mathematical analysis simulation results are not specific numbers but functions. The tree safety factor is the ratio of the critical tree height (H_{cr}) to the actual tree height (H), as expressed in Equation 34. A tree is considered safe if the resulting S_f value is greater than 1 and meets the requirements for load combinations.

$$S_f = \frac{H_{cr}}{H} \quad (34)$$

RESULTS AND DISCUSSION

Characteristics of trees

The morphometric characteristics of the rain trees are presented in Table 1. The average total height of the rain tree is 25.93 meters, at branch-free height is 2.84 meters, the lowest crown height is 9.28 meters, the crown height is 16.65 meters, the Diameter at breast height (Dbh) is 59.65 centimeters, the tip diameter is 52.20 centimeters and crown diameter (Dc) is 8.70 meters. This is consistent with Karlinasari et al. (2021, 2023), who found in their study that the D_{bh} of rain trees ranges from 35.7 to 116 cm. Rahardjo et al. (2014) and Mardiatmoko (2016) reported that the tree height can reach 15-30 m with the crown diameter often being wider than the height of the tree. The characteristics of trembesi align with the characteristics of a decurrent tree, which typically has a short main trunk and spreading crown (Coder 2014; Li et al. 2022). Tree growth is influenced by several factors, including light, temperature, precipitation, drought, soil moisture, silvicultural treatment, genetics, and hormones (Harvey et al. 2019). Other studies also mention that tree size and growth rate are influenced by wind, which has an impact on carbon stock and storage (Bonnesoeur et al. 2016; MacFarlane and Kane 2017).

The taper and slenderness values of the rain trees in the research site are listed in Table 2. Stem tapering is the degree of change (decrease rate) in the stem diameter from a certain point (ground level) to the tip (Yang and Burkhart 2020; Seki 2023). The stem taper has an important role in forest management, forest planning, forest inventory, and growth projection (Salekin et al. 2021). It is also an important parameter for determining the critical height of trees for preventing buckling (Dargahi et al. 2019). Karlinasari et al. (2023) explained that the larger the taper value, the more tapered the tree stems. The taper value for the rain tree was 0.10, for the agathis tree was 0.71, and for the royal palm was 0.38 (Karlinasari et al. 2023). However, in the present study, the taper value for rain trees was 0.12. This indicates that the rain tree stem has a less tapered characteristic than the agathis and royal palm trees. Therefore, rain trees have a lower risk in terms of buckling of the main stem (Karlinasari et al. 2023). Factors influencing the shape of tree stems include tree positioning and spacing, soil density, plant maintenance, fertilization, and genetic factors (McTague and Weiskittel 2020). The slenderness coefficient of the tree stems (slenderness or S) based on morphometry was defined as the ratio of tree length (branch-free height) to D_{bh}. The average slenderness value of the tree stems based on morphometry was 5.57. Trees with low slenderness typically have larger canopies, more developed root systems, and less slender or tapered stems (Karlinasari et al. 2021). Factors that influence slenderness include silvicultural treatment, stand age, stand density, crown width, soil type, slope, and nutrient content (Zhang et al. 2020).

The modulus of elasticity (*MoE* or *E*) is a parameter used to determine the corrected compression stress in wood or trees (AWC 2018). This value was used in cooperating to calculate the tree stability (Karlinasari et al. 2021). The static modulus (*Es*) used in the calculation was generated by the dynamic *E*, which was obtained from field testing using a non-destructive testing tool for measuring sound wave propagation from a tree stem (Duong and Schimleck 2022). Wood density was determined in cooperation with stem weight. The values are presented in Table 3. The results show that the average density of fresh rain tree stems is 1107.69 kg m^{-3}, the sound wave velocity is 2768.60 m s^{-1}, and the static *E* (E_s) is 4.95 GPa. This aligns with Karlinasari et al. (2021), who reported that the sound wave velocity in rain tree stems ranges from 1787.72 to 3334.53 m s^{-1}. However, for wood density and E_s, this research indicates higher values compared to Karlinasari et al. (2023), which reported wood density and static *E* values for rain trees as 778.20 kg m^{-3} and 3.89 GPa, respectively. Thus, the *E* value of wood can indicate the stiffness. The stiffness can affect the stability of the tree because if the tree grows taller without increasing its stiffness, the tree may fall under its weight. The reason is that it is unable to withstand the load that occurs (Moulia et al. 2019). Therefore, the larger the *E* value, the stiffer the wood, and the smaller the risk of deflection and bending (Karlinasari et al. 2023). In addition, *MOE* determines a material's strength based on how much it can withstand deformation when forced under load during a bending test (Vaughan et al. 2021). This study opens up exciting possibilities for further exploration and discovery in the field of wood science and tree stability.

Table 1. The characteristics of the rain trees

Parameter	Symbol	Unit	Rain tree (n = 50)		
			Average	St.Dev	CV
Total tree height	H	m	25.93	7.34	0.28
Branch-free height	H_{tbc}	m	2.84	1.56	0.55
Lowest crown height	H_{ck}	m	9.28	4.92	0.53
Crown height	H_c	m	16.65	7.03	0.42
Diameter at breast height	D_{bh}	cm	59.65	19.92	0.33
Tip diameter	D_{tr}	cm	52.20	17.90	0.34
Average crown diameter	D_c	m	8.70	2.86	0.33

Table 2. The values of tapered and slenderness of the rain trees

Parameter	Symbol	Unit	Rain tree (n = 50)		
			Average	St.Dev	CV
Taper of stems	T	ratio	0.12	0.08	0.61
Slenderness of stems	S	ratio	5.57	5.05	0.91

Table 3. The value of average wood density, sound wave velocity, and static modulus of elasticity of the rain trees

Parameter	Symbol	Unit	Rain tree (n = 50)		
			Average	St.Dev	CV
Fresh wood density	ρ	kg m^{-3}	1107.69	165.51	0.15
Sound wave velocity	S_{WVT}	m s^{-1}	2768.60	357.16	0.13
Static *MoE*	E_s	GPa	4.95	1.43	0.29

Table 4. The average critical height trees of the rain trees

Load condition	Actual height	Critical height	Difference
Combination (compression and bending)	25.93	28.26	2.33
Combination compression (internal dan external)	25.93	36.53	10.61
Internal compression	25.93	36.91	10.98

Table 5. Conditions of rain trees based on safety factors

Tree condition	*Safety factor*	Number of trees	Percentage (%)
Unsafe	$S_f \leq 1$	18	36
Safe	$1 < S_f \leq 1.645$	30	60
Very safe	$S_f > 1.645$	2	4

Stress analysis and critical height of trees

The critical height of a tree is determined to indicate the maximum height that the tree can withstand before bending (Karlinasari et al. 2023). The critical height was determined by simulating the loads applied to the tree using the Desmos Graphic Calculator (see Figures 5, 6, and 7). Each tree was simulated for three critical height values based on the loading conditions, i.e., H_{cr1} for the first loading condition (combined load of compression and bending or D + L + W), H_{cr2} for the second loading condition (combined internal and external compression loads or D + L), and H_{cr3} for the third loading condition (internal compression load or *D*). The average simulation values for each critical height, relative to the actual tree height, are listed in Table 4.

The study results showed that the minimum difference in the critical height value of the tree was obtained from the first loading condition, namely the combination of compression and bending loads. This suggests that the minimum critical height value is always derived from the D + L + W combined load condition, resulting in a superposition of the resultant compression and bending stresses. For that reason, the wind load is a limiting condition for tree stability. Trees subjected to wind loads with their own weight and live load (D + L + W) are less safe than trees subjected to only their weight (D). This is also following James (2014), Yang et al. (2014), Jackson et al. (2021), Kitenberga et al. (2021), and Amani-Beni et al. (2023), which show that wind is an important parameter that affects the structural stability of trees. Table 4 shows three critical height values based on loading conditions. The minimum critical height value (H_{cr1}) (with the smallest difference from the actual value) was selected and used to determine the safety factor. This value is the maximum height limit of the tree that can withstand the acting load. If the tree's height exceeds the critical height when subjected to the same load, the tree will buckle until failure. In addition, the implication of this finding to urban forestry management can be used to determine the critical height of trees in terms of the load from the tree crown. This information can be combined with tree maintenance activities, especially for pruning or other justifications for tree arrangement.

Tree safety factor

The safety factor (S_f) is a dimensionless ratio, meaning that the divided quantities should have the same units, such as load, height, and speed (Kadry et al. 2019). It is also one of the parameters that can be used to determine tree safety and risk rating (Helmanto et al. 2022), as well as to determine the mechanical load acting on the tree objectively. This study determined the safety factor based on total height (H) and critical tree height (H_{cr}). The tree conditions were classified into three categories based on the safety factor values. First, a tree was considered unsafe if $S_f \leq 1$. Second, a tree was considered safe if $1 < S_f \leq 1.645$. Third, a tree was considered safe if $S_f > 1.645$ (Karlinasari et al. 2023). The conditions of the rain tree are listed in Table 5. According to these data, there were 18 unsafe trees, 30 safe trees, and 2 very safe trees. Representative graphic-mathematical analysis images for each tree condition and loading condition are shown in Figures 5, 6, and 7. A study by Kadry et al. (2019) has developed the safety factor (S_f) where $S_f < 1$ indicates unsafety with the explanation as a risk of damage such as breaking or toppling. S_f values between 1 and 1.5 are considered safe, but measures such as crown pruning are necessary to prevent damage. A value of $S_f > 1.5$ indicates very safe conditions. The S_f value can reach three ($S_f > 3$) or higher in an ideal scenario for healthy trees.

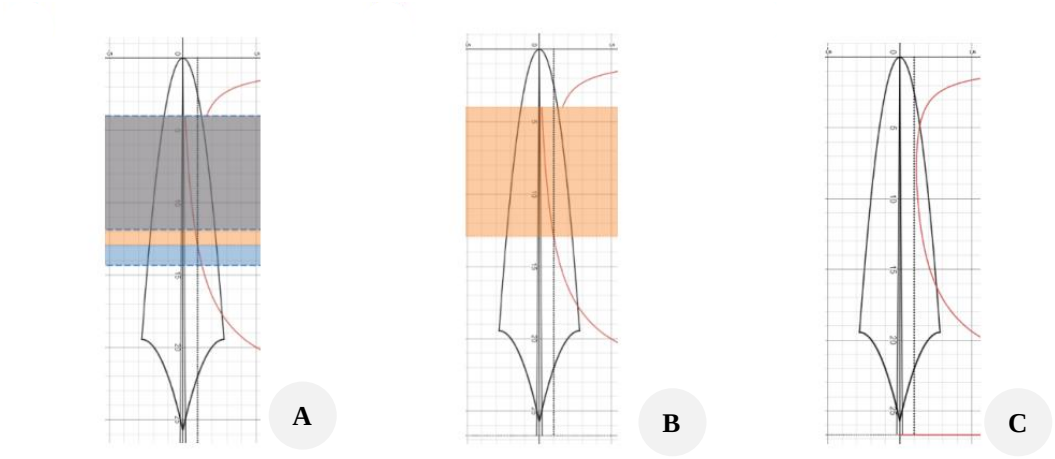

Figure 5. Determination of critical buckling height (H_{cr}) using a simulation from the Desmos graphical calculator. Graphic-mathematical analysis of unsafe tree conditions at: A. Combined load; B. Internal and external compression load; C. Internal compression load. The red line is compression ratio from ($L(x)$) to ($G(x)$), the orange area appear if the S_f greater than compression ratio, the blue area appear if the combined load greater than 1, and the dotted line is a safety factor line $S_f = 1$. (Notes: The x-axes represent the tree height from the tip ($x = 0$ m) to the base or ground ($x = H$ m); meanwhile, the y-axes represent the threshold for tree safety factor)

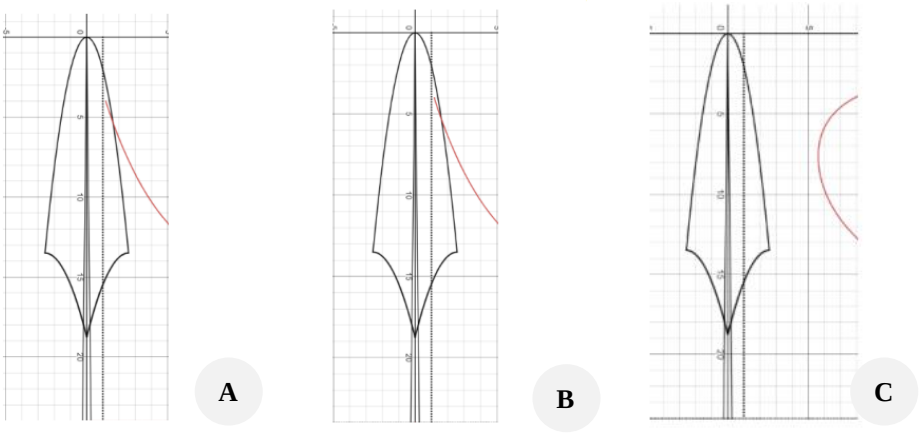

Figure 6. Determination of critical buckling height (H_{cr}) using a simulation from the Desmos graphical calculator. Graphic-mathematical analysis of safe tree conditions at: A. Combined load; B. Internal and external compression load; C. Internal compression load. The red line is compression ratio from ($L(x)$) to ($G(x)$), and the dotted line is a safety factor line $S_f = 1$. (Notes: The x-axes represent the tree height from the tip ($x = 0$ m) to the base or ground ($x = H$ m); meanwhile, the y-axes represent the threshold for tree safety factor)

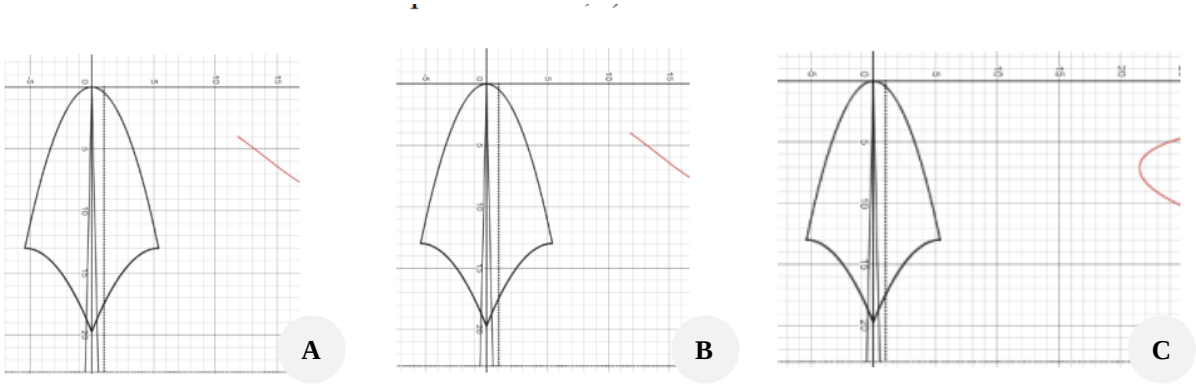

Figure 7. Determination of critical buckling height (H_{cr}) using a simulation from the Desmos graphical calculator. Graphic-mathematical analysis of very safe tree condition at: A. Combined load; B. Internal and external compression load; C. Internal compression load. The red line is compression ratio from ($L(x)$) to ($G(x)$), and the dotted line is a safety factor line $S_f = 1$. (Notes: The x-axes represent the tree height from the tip ($x = 0$ m) to the base or ground ($x = H$ m); meanwhile, the y-axes represent the threshold for tree safety factor)

This study is very helpful in analyzing the ability of tree trunks to bear the "load" both from their own load (crown and mass of tree trunk wood) and external loads (wind factors). In this case, it can refer to regardless of species, as long as the structural parameters such as height, diameter, and density (wood and crown) are known, so that these parameters can then be used in calculating the structural analysis. The structural equations presented and the use of the Desmos calculation tool in the study are very common and well-known to engineers, which can help apply the structure calculation following SNI (2013). Therefore, it is hoped that this study can be a bridge for research collaboration between engineers and biologists in terms of biomechanics study.

In conclusion, the mechanical stability of a tree can be assessed through structural analysis by considering the effects of compressive and bending loads acting on the tree. Growth characteristics, such as tree height, crown height and diameter, D_{bh}, and various other parameters, are crucial for determining these loads. Additionally, choosing the critical height of the tree is very important to determine the value of the safety factor and the overall tree condition. Based on the safety factor value, 2 trees (4%) are categorized as very safe. In addition, the majority of trees are in safe condition (30 trees or 60%); however, 18 trees (36%) are included in the unsafe category. This indicates that the wind load and external factors, such as people climbing the tree, affect the capacity of the tree to resist bending (tree stability). In the next study, root characteristics and environmental factors beyond wind load, such as soil conditions, can be included as the factors affecting tree stability.

ACKNOWLEDGEMENTS

This research was funded by a Competitive Grant from the Ministry of Education, Culture, Research, and Technology, Republic of Indonesia, for FY 2023, through the research topic of Tree Biomechanics, with contract number: 001/E5/PG.02.00.PL/2023 and 15856/IT3.D10/PT.01.02/P/T/2023.

REFERENCES

Afrianto WF, Wati SI, Hidayatullah T. 2021. The suitability assessment of the tree species in the urban parks and urban forest in Kediri City, East Java, Indonesia. Nusantara Biosci 13 (2): 131-139. DOI: 10.13057/nusbiosci/n130201.

Amani-Beni M, Malazi MT, Dehghanian K, Dehghanifarsani L. 2023. Investigating the efects of wind loading on three dimensional tree models using numerical simulation with implications for urban design. Sci Rep 13 (1): 7277. DOI: 10.1038/s41598-023-34071-5.

America Wood Council (AWC). 2018. National Design Specification (NDS) for wood construction. American Wood Council, Virginia.

American Society for Testing and Materials (ASTM). 2002. ASTM D245-00: Standard Practice for Establishing Structural Grades and Related Allowable Properties for Visually Graded Lumber. ASTM Committee, Philadelphia.

American Society for Testing and Materials (ASTM). 2017. ASTM D2395-17: Standard Test Methods for Density and Specific Gravity (Relative Density) of Wood and Wood-Based Materials. ASTM Committee, Philadelphia.

Badel E, Ewers FW, Cochard H, Telewski FW. 2015. Acclimation of mechanical and hydraulic functions in trees: Impact of the thigmomorphogenetic process. Front Plant Sci 6: 266. DOI: 10.3389/fpls.2015.00266.

Bonnesoeur V, Constant T, Moulia B, Fournier M. 2016. Forest trees filter chronic wind-signals to acclimate to high winds. New Phytol 210 (3): 850-860. DOI: 10.1111/nph.13836.

Borisevich SA, Vikhrenko VS. 2018. Evaluation of the drag coefficients of tree crowns by numerical modeling of their free fall. Agric For Meteorol 256-257: 346-352. DOI: 10.1016/j.agrformet.2018.03.020.

Cardia F, Lovatelli A. 2015. Aquaculture Operations in Floating HDPE Cages (A Field Handbook). FAO and Ministry of Agriculture of the Kingdom of Saudi Arabia, Rome.

Central Bureau of Statistics (BPS). 2022. Wind Speed in Bogor in 2022. BPS. https://bogorkota.bps.go.id/subject/151/iklim.html

Coder KD. 2014. Advanced Tree Biology: Tree Anatomy. University of Georgia, Atlanta.

Dahle G, Grabosky J, Kane B, Miesbauer J, Peterson W, Telewski FW, Koeser A, Watson GW. 2014. Tree biomechanics: A white paper from the 2012 international meeting and research summit at the morton arboretum (Lisle, Illinois, U.S.). Arboric Urban For 40 (6): 309-318. DOI: 10.48044/jauf.2014.029.

Dargahi M, Newson T, Moore J. 2019. Buckling behaviour of trees under self-weight loading. Forestry 92 (4): 393-405. DOI: 10.1093/forestry/cpz027.

Directorate General of Highways. 1996. Guidelines for Road Landscape Planning. Ministry of Public Works, Jakarta. [Indonesian]

Duong DV, Schimleck L, Lam TD, Vo HD. 2022. Radial and among-clonal variation of stress-wave velocity, wood density, and mechanical properties in 5-year-old acacia auriculiformis clones. BioResources 17: 2084-2096. DOI: 10.15376/biores.17.2.2084-2096.

Duong DV, Schimleck L. 2022. Prediction of static bending properties of *Eucalyptus* clones using stress wave measurements ons tanding trees, logs, and small clear specimens. Forest 13 (10): 1728. DOI: 10.3390/f13101728.

Fathi S. 2020. The Reability and Application of Dynamic Tree Stability Inspection. [Dissertation]. University of Sopron, Hungary.

Forest Products Laboratory. 2010. Wood Handbook: Wood as an Engineering Material. United States Department of Agriculture Forest Service, Wisconsin.

Fournier M, Almeras T, Clair B, Gril J. 2013. Biomechanical actions and biological function. In: Gardiner B, Barnett J, Saranpää P, Gril J (eds). The Biology of Reaction Wood. Springer Series in Wood Science. Springer, Berlin. DOI: 10.1007/978-3-642-10814-3_5.

Fundova I, Funda T, Wu HX. 2019. Non-destructive assessment of wood stiffness in Scots pine (*Pinus sylvestris* L.) and its use in forest tree improvement. Forests 10 (6): 491. DOI: 10.3390/f10060491.

Gardiner B, Berry P, Moulia B. 2016. Review: Wind impacts on plant growth, mechanics and damage. Plant Sci 245: 94-118. DOI: 10.1016/j.plantsci.2016.01.006.

Gonçalves R, Linhares C, Yojo T. 2020. Drag coefficient in urban trees. Trees 37: 133-145. DOI: 10.1007/s00468-019-01951-1.

Harvey JE, Smiljanić M, Scharnweber T et al. 2019. Tree growth influenced by warming winter climate and summer moisture availability in northern temperate forests. Glob Change Biol 26 (4): 2505-2518. DOI: 10.1111/gcb.14966.

Helmanto H, Damayanti F, Rachmadiyanto AN. 2022. A safety factor old trees *Pterocarpus indicus* Willd. in Bogor Botanic Gardens. IOP Conf Ser: Earth Environ Sci 950: 012009. DOI: 10.1088/1755-1315/950/1/012009.

Horváthová E, Badura T, Duckhova H. 2021. The value of the shading function of urban trees: A replacement cost approach. Urban For Urban Green 62: 127166. DOI: 10.1016/j.ufug.2021.127166.

Hui KKW, Wong MS, Kwok CYT, Li H, Abbas S, Nichol JE. 2022. Unveiling falling urban trees before and during Typhoon Higos (2020): Empirical case study of potential structural failure using Tilt Sensor. Forest 13 (2): 359. DOI: 10.3390/f13020359.

Iizuka K, Yonehara T, Itoh M, Kosugi Y. 2018. Estimating tree height and Diameter at Breast Height (DBH) from digital surface models and orthophotos obtained with an unmanned aerial system for a Japanese Cypress (*Chamaecyparis obtusa*) Forest. Remote Sens 10 (1): 13. DOI: 10.3390/rs10010013.

Indonesian National Standard (SNI). 2013. SNI 7973: Design Specifications for Timber Structures. National Standardization Agency, Jakarta. [Indonesian]

International Organization for Standardization (ISO). 1975. ISO 2533-1975: Standard Atmosphere. ISO Technical Committee, Switzerland.

Jackson TD, Sethi S, Dellwik E. 2021. The motion of trees in the wind: A data synthesis. Biogeosciences 18 (13): 4059-4072. DOI: 10.5194/bg-18-4059-2021.

Jackson TD, Shenkin AF, Majalap N, Bin Jami J, Bin Sailim A, Reynolds G, Coomes DA, Chandler CJ, Boyd DS, Burt A, Wilkes P, Disney M, Malhi Y. 2020. The mechanical stability of the world's tallest broadleaf trees. Biotropica 53 (1): 110-120. DOI: 10.1111/btp.12850.

James K. 2014. Tree stability in wind storms-Open grown trees in urban areas. Arboricultural Association's 48th Annual Amenity Arboriculture Conference. Royal Holloway, University of London. 14-17 September 2014. DOI: 10.13140/2.1.4295.5525.

Jansson M. 2014. Green space in compact cities: The benefits and values of urban ecosystem services in planning. Nord J Arch Res 2: 139-160.

Kadry D, Divos F, Buza AK, Bejo L, Kolarik J. 2019. Tree assessor-instrumental tree assessment advance-tree assessment-manual for professional. Dobre Kadry Research and Training Center, Ltd./ Fakkop Enterprise, Wroclaw.

Karlinasari L, Adzkia U, Puspitasari T, Nandika D, Nugroho N, Syafitri UD, Siregar IZ. 2021. Tree morphometric relationships and dynamic elasticity properties in tropical rain trees (*Samanea saman* Jacq. Merr). Forest 12 (12): 1711. DOI: 10.3390/f12121711.

Karlinasari L, Bahtiar ET, Kadir ASA, Adzkia U, Nugroho N, Siregar IZ. 2023. Structural analysis of self-weight loading standing trees to determine critical buckling height. Sustainability 15 (7): 6075. DOI: 10.3390/su15076075.

Kitagawa K, Iwama S, Fukui S, Sunaoka Y, Yazawa H, Usami A, Naramoto M, Uchida T, Saito S, Mizunaga H. 2015. Effects of components of the leaf area distribution on drag relations for *Cryptomeria japonica* and *Chamaecyparis obtusa*. Eur J For Res 134: 403-414. DOI: 10.1007/s10342-014-0859-6.

Kitenberga M, Šņepsts G, Vuguls J, Elferts D, Jaunslaviete I, Jansons Ā. 2021. Tree- and stand-scale factors shape the probability of wind damage to birch in hemiboreal forests. Silva Fennica 55 (2): 10483. DOI: 10.14214/sf.10483.

Koizumi A, Shimizu M, Sasaki Y, Hirai T. 2016. In situ drag coefficient measurements for rooftop trees. J Wood Sci 62: 363-369. DOI: 10.1007/s10086-016-1556-5.

Li F, Liu X, Zhang X, Zhao D, Liu H, Zhou C, Wang R. 2016. Urban ecological infrastructure: An integrated network for ecosystem services and sustainable urban systems. J Clean Prod 163 (S1): S12-S18. DOI: 10.1016/j.jclepro.2016.02.079.

Li Z, Hao Y, Kopp GA, Wu C-H. 2022. Identification of multimodal dynamic characteristics of a decurrent tree with application to a model-scale wind tunnel study. Appl Sci 12 (15): 7432. DOI: 10.3390/app12157432.

Linhares CSF, Gonçalves R, Martins LM, Knapic S. 2021. Structural stability of urban trees using visual and instrumental techniques: A review. Forest 12 (12): 1752. DOI: 10.3390/f12121752.

MacFarlane DW, Kane B. 2017. Neighbour effects on tree architecture: functional trade-offs balancing crown competitiveness with wind resistance. Funct Ecol 31 (8): 1624-1636. DOI: 10.1111/1365-2435.12865.

Manickathan L, Defraeye T, Allegrini J, Derome D, Carmeliet J. 2018. Comparative study of flow field and drag coefficient of model and small natural trees in a wind tunnel. Urban For Urban Green 35: 230-239. DOI: 10.1016/j.ufug.2018.09.011.

Mardiatmoko G. 2016. Allometric equations for predicting above and below-ground biomass of young rain tree [*Albizia saman* (jacq.) Merr.] to handle climate change. Asian J Microbiol Biotechnol Environ Sci 18 (4): 821-830.

McTague JP, Weiskittel A. 2020. Evolution, history, and use of stem taper equations: A review of their development, application, and implementation. Can J For Res 51: 210-235. DOI: 10.1139/cjfr-2020-0326.

Miyashita A, Suzuki S. 2021. A method for measuring the forces acting on a tree trunk using strain gauges. PLoS One 16 (1): e0245631. DOI: 10.1371/journal.pone.0245631.

Moore J, Gardiner B, Sellier D. 2018. Tree mechanins and wind loading. In: Geitmann A, Gril J (eds). Plant Biomechanics. Springer, Cham. DOI: 10.1007/978-3-319-79099-2_4.

Moulia B, Bastien R, Chauvet-Thiry H, Leblance-Fournier N. 2019. Posture control in land plants: Growth, position sensing, proprioception, balance, and elasticity. J Exp Bot 70 (14): 3467-3494. DOI: 10.1093/jxb/erz278.

Mulyasari I, Purbowati. 2018. Upper arm circumference and ulnar length were used as anthropometric parameters to estimate the body weight and height of adults. Jurnal Gizi Indonesia 7 (1): 30-36. DOI: 10.14710/jgi.7.1.30-36. [Indonesian]

Němec P. 2015. Comparison of modern forest inventory method with the common method for management of tropical rainforest in the Peruvian Amazon. J Trop For Sci 27 (1): 80-91.

O'Brien L, De Vreese R, Kern M, Sievänen T, Stojanova B, Atmiş E. 2017. Cultural ecosystem benefits of urban and peri-urban green infrastructure across different European countries. Urban For Urban Green 24: 236-248. DOI: 10.1016/j.ufug.2017.03.002.

Ow LF, Ghosh S, Yusof MLM. 2019. Growth of *Samanea saman*: Estimated cooling potential of this tree in an urban environment. Urban For Urban Green 41: 264-271. DOI: 10.1016/j.ufug.2019.03.021.

Ow LF, Ghosh S. 2017. Urban tree growth and their dependency on infiltration rates in structural soil and structural cells. Urban For Urban Green 26: 41-47. DOI: 10.1016/j.ufug.2017.06.005.

Ow LF, Yusof MLM. 2018. Stability of four urban tree species in engineered and regular urban soil blends. J Urban Ecol 4 (1): juy014. DOI: 10.1093/jue/juy014.

Palace MW, Sullivan FB, Ducey MJ, Treuhaft RN, Herrick C, Shimbo JZ, Mota-E-Silva J. 2015. Estimating forest structure in a tropical forest using field measurements, a synthetic model and discrete return lidar data. Rem Sens Environ 161: 1-11. DOI: 10.1016/j.rse.2015.01.020.

Puspitasari T. 2021. Biomechanics of the Rain Tree (*Samanea saman* (Jacq.) Merr) in the IPB Dramaga Campus Landscape: Morphometric, Visual, and Mechanical Analysis. [Bachelor's thesis]. IPB, Bogor. [Indonesian]

Rahardjo H, Harnas FR, Indrawan IGB, Leong EC, Tan PY, Fong YK, Ow LF. 2014. Understanding the stability of *Samanea saman* trees through tree pulling, analytical calculations and numerical models. Urban For Urban Green 13 (2): 355-364. DOI: 10.1016/j.ufug.2013.12.002.

Salekin S, Catalán CH, Boczniewicz D, Phiri D, Morgenroth J, Meason DF, Mason EG. 2021. Global tree taper modelling: A review of applications, methods, functions, and their parameters. Forests 12 (7): 913. DOI: 10.3390/f12070913.

Schimleck L, Dahlen J, Apiolaza LA, Downes G, Emms G, Evans R, Moore J, Pâques L, Van den Bulcke J, Wang X. 2019. Non-destructive evaluation techniques and what they tell us about wood property variation. Forests 10 (9): 728. DOI: 10.3390/f10090728.

Seki M. 2023. Predicting stem taper using artificial neural network and regression models for Scots pine (*Pinus sylvestris* L.) in northwestern Türkiye. Scandinavian J For Res 38 (1-2): 97-104. DOI: 10.1080/02827581.2023.2189297.

Spatz H-C, Bruechert F. 2000. Basic biomechanics of self-supporting plants: Wind and gravitational loads on *Norway spruce* trees. For Ecol Manag 135 (1-3): 33-44. DOI: 10.1016/S0378-1127(00)00296-6.

Telewski FW, Moore JR. 2016. Trait selection to improve wind-firmness in trees. CABI Rev 11 (050): 1-10. DOI: 10.1079/pavsnnr201611050.

Tiwary A, Williams ID, Heidrich O, Namdeo A, Bandaru V, Calfapietra C. 2016. Development of multi-functional streetscape green infrastructure using a performance index approach. Environ Pollut 208 (Pt A): 209-220. DOI: 10.1016/j.envpol.2015.09.003.

Urhan OS, Kolpak SE, Jayawicakrama KJS, Howe GT. 2014. Early genetic selection for wood stiffness in juvenile Douglas-fir and western hemlock. Forest Ecology and Management 320: 104-117. DOI: 10.1016/j.foreco.2014.02.020.

Vaughan D, Auty D, Dahlen J, Meador AJS, Mackes KH. 2021. Modeling variation in wood stiffness of *Pinus ponderosa* using static bending and acoustic measurements. Forestry: Intl J For Res 94 (2): 232-243. DOI: 10.1093/forestry/cpaa030.

Ver Planck NR, MacFarlane DW. 2019. Branch mass allocation increases wind throw risk for *Fagus grandifolia*. Forestry: Intl J For Res 92 (4): 490-499. DOI: 10.1093/forestry/cpz001.

Wolf KL, Lam ST, McKeen JK, Richardson GRA, van den Bosh M, Bardekjian AC. 2020. Urban trees and human health: A scooping review. Intl J Environ Res Public Health 17 (12): 4371. DOI: 10.3390/ijerph17124371.

Yang M, Défossez P, Danjon F, Fourcaud T. 2014. Tree stability under wind: simulating uprooting with root breakage using a finite element method. Ann Bot 114 (4): 695-709. DOI: 10.1093/aob/mcu122.

Yang S-I, Burkhart HE. 2020. Robustness of parametric and nonparametric fitting procedures of tree-stem taper with alternative definitions for validation data. J For 118 (6): 576-583. DOI: 10.1093/jofore/fvaa036.

Zhang X, Wang H, Chhin S, Zhang J. 2020. Effects of competition, age, and climate on the tree slenderness of Chinese fir plantations in Southern China. For Ecol Manag 458: 117815. DOI: 10.1016/j.foreco.2019.117815.